Precipitation Kinetics in a Nb-stabilized Ferritic Stainless Steel

M. LABONNE, A. GRAUX, S. CAZOTTES, F. DANOIX, F. CUVILLY, F. CHASSAGNE, M. PEREZ, and V. MASSARDIER

The precipitation occurring in a Nb-stabilized ferritic stainless steel, containing initially Nb(C, N) carbonitrides and Fe_3Nb_3X precipitates, was investigated during aging treatments performed between 923 K and 1163 K (650 °C and 890 °C) by combining different techniques, (thermoelectric power (TEP), scanning/transmission electron microscopy (SEM/TEM), and atom probe tomography (APT)), in order to determine the precipitation kinetics, the nature and morphology of the newly formed precipitates as well as the chemistry of the initial Fe_3Nb_3X precipitates, where X stands for C or N. The following composition was proposed for these precipitates: $(Fe_{0.81}\ Cr_{0.19})_3\ (Nb_{0.85}\ Si_{0.08}\ Mo_{0.07})_3\ (N_{0.8}\ C_{0.2})$, highlighting the simultaneous presence of N and C in the precipitates. With regard to the precipitation in the investigated temperature range, two main phenomena, associated with a hardness decrease, were clearly identified: (i) the precipitation of Fe_2Nb precipitates from the niobium initially present in solution or coming from the progressive dissolution of the Fe_3Nb_3X precipitates and (ii) the precipitation of the χ-phase at grain boundaries for longer aging times. From the TEP kinetics, a time–temperature–precipitation diagram has been proposed.

DOI: 10.1007/s11661-017-4158-y

I. INTRODUCTION

IN the last 15 years, austenitic stainless steels have been gradually replaced by ferritic stainless steels in automotive exhaust systems, for which the temperature of the exhaust gas tends to be increased above 1173 K (900 °C) for fuel economy and for cleaning the gas emissions.[1–6] Ferritic stainless steels present several advantages. First, they are not subjected to the fluctuation of nickel price. Second, during thermal cycles, ferritic grades are characterized by a much smaller thermal dilatation than austenitic grades, leading to a reduction of the stresses between the metal and the oxide layer developed on its surface. Consequently, fewer cracks are formed in the oxide layer and the oxide barrier remains more continuous, decreasing the oxidation kinetics.[1] However, ferritic grades have poorer mechanical properties in terms of high temperature strength,[2,3,5,7] which is detrimental for their resistance to thermal fatigue.

This is the reason for which niobium is commonly added in ferritic stainless steels, due to its positive influence on mechanical properties.[1–5,7] Strength at elevated temperature can be substantially improved with the addition of niobium through solid solution and/or precipitation strengthening. In particular, grain boundary precipitation may occur, leading to an improved creep resistance.[7] Furthermore, the addition of small amounts of niobium in ferritic stainless steels was found to lead to a general grain refinement in the as-cast microstructures.[8] Lastly, niobium prevents the precipitation of $Cr_{23}C_6$ chromium carbides at grain boundaries. The formation of these carbides is believed to be deleterious because it leads to a depletion of the chromium content of the matrix surrounding the grain boundaries in which chromium carbides have formed[9]: this can result in a poor resistance to intergranular corrosion if the local composition of chromium falls below the critical value of 12 pct. When niobium is added, carbon reacts preferentially with this element rather than with chromium, preventing the risk of intergranular corrosion.[10]

In the literature,[2–5,7,10–13] three types of precipitates have been identified as playing a role in the strengthening mechanisms of Nb-stabilized ferritic stainless steels: Nb(C, N) (carbonitride), Fe_2Nb (Laves phase), and Fe_3Nb_3X (M_6C carbide), where X stands for C or N.

M. LABONNE, A. GRAUX, S. CAZOTTES, M. PEREZ, and V. MASSARDIER are with the Univ. Lyon, INSA Lyon, MATEIS UMR CNRS 5510, Bât. Saint-Exupéry, 25 avenue J. Capelle, 69621 Villeurbanne Cedex, France. Contact e-mail: veronique.massardier@insa-lyon.fr F. DANOIX and F. CUVILLY are with the Normandie Univ, UNIROUEN, INSA Rouen, CNRS, Groupe de Physique des Matériaux, 76000 Rouen, France. F. CHASSAGNE is with the APERAM Research Center, BP15, 62330 Isbergues, France.
Manuscript submitted March 13, 2017.

Published online: 31 May 2017

However, two main points currently need to be addressed and will be discussed in the present paper. The first point concerns the stability domains and the precipitation kinetics of the phases, which were not clearly established in the literature due to the complexity of Nb-stabilized ferritic stainless steels. The second point that still needs to be clarified is the exact nature of Fe_3Nb_3X precipitates, especially the nature of the light element X. This phase has been successively characterized as follows: (i) Fe_2Nb_3 by Chassagne *et al.*[7] with energy-dispersive spectroscopy (EDS) and selected area electron diffraction (SAED), (ii) Fe_3Nb_3C by Fujita *et al.*[3] with the same techniques, and (iii) Fe_3Nb_3N by Malfliet *et al.*[11] with auger electron spectroscopy (AES). This latter study suggests that the chemistry measurements, involving the presence of C and/or O atoms, could be due to the contamination of samples by these elements.

The investigations on these two points are of great importance, considering that mechanical properties are affected by the nature, size, volume fraction, and localization of the precipitates. This requires an accurate description of the precipitation kinetics of the different types of precipitates, in order to be able to predict the mechanical properties of the material.

With regard to the precipitation kinetics, the results of the literature[2–5,7] are rare and give only some tendencies. According to the works of Sim *et al*,[5] the three types of precipitates (Nb(C, N), Fe_2Nb, and Fe_3Nb_3X) can be detected during aging at 973 K (700 °C) of Fe-15Cr-*y*Nb-0.01C steels with $0.38 < y < 0.8$ wt. pct. In these steels, the simultaneous presence of the Fe_2Nb Laves phase and of Nb(C, N) carbonitride was noted for short treatment times (30 and 120 minutes). For longer treatment times (1000 hours), Fe_3Nb_3X precipitates were also highlighted. The results of Fujita *et al.*[3] on a Fe-13Cr-0.5Nb-0.01C steel support the coexistence of the three types of precipitates after a long holding time (100 hours) at 1073 K, 1123 K, and 1173 K (800 °C, 850 °C, and 900 °C) and show that the amount of Fe_3Nb_3X tends to become predominant at longer times and higher temperature. This latter result is in agreement with the works of Malfliet *et al.*[12] which suggests that Fe_3Nb_3X tends to form by destabilizing Nb(C, N) around 1273 K (1000 °C). However, it has already been shown that the presence of other alloying elements (Mo, Ti) in the steel composition may modify significantly the precipitation sequence.[3]

Concerning the exact nature of the Fe_3Nb_3X precipitates, the discrepancies between authors can be partly explained by the fact that the spatial resolution of the techniques used for the analysis of the precipitates is of the order of 1 μm for selected area electron diffraction (SAED) and energy-dispersive spectroscopy (EDS),[14] and 50 nm for auger electron spectroscopy (AES).[15] This resolution is not sufficient for the study of Fe_3Nb_3X precipitates, the size of which is between 50 and 300 nm. Hence, the response of these techniques is not only due to the precipitates themselves but also to the surrounding matrix, which makes the study of small precipitates by these techniques inaccurate. Consequently, the determination of nature of the light element is a difficult task using classical electron microscopy tools.

In the aforementioned context, the present work aims at: (i) following the precipitation kinetics of the different phases formed in an industrial Fe-19Cr-0.57Nb-0.01C-0.02N steel (containing also other alloying elements such as Mo, Mn, Ni, Si) between 923 K and 1173 K (650 °C to 900 °C) by coupling thermoelectric power (TEP) measurements with transmission electron microscopy (TEM) observations and (ii) determining the composition of the Fe_3Nb_3X precipitates using atom probe tomography (APT). Lastly, the effects of the precipitation on the mechanical properties will be investigated through Vickers hardness measurements.

II. MATERIAL AND EXPERIMENTAL PROCEDURE

A. *Material*

The composition of the ferritic stainless steel investigated in this work is presented in Table I. The ''as-received'' condition of the steel was obtained by casting and hot rolling to a thickness of 5 mm. The hot-rolled samples were then annealed at 1323 K (1050 °C) for a few seconds and air-cooled. In order to study precipitation in the investigated steel, the samples were subsequently treated at a given temperature [between 923 K and 1163 K (650 °C and 890 °C)] for different treatment times (from 0 to 2 hours). These treatments were performed to determine the phases, which can be encountered during cooling after hot rolling or during high temperature exposure.

For short treatment times (less than or equal to 30 minutes), the samples were treated in a salt bath and subsequently, water-quenched. For longer treatments, they were treated in vacuumed quartz capsules to avoid any undesirable interaction between the sample and the salt bath. Due to the difficulty in quenching the samples inserted in the quartz capsules, after their long treatment at a given temperature, they were re-introduced in a salt bath for 30 seconds at the same temperature and then, water-quenched. This was performed in order to prevent any precipitation phenomenon, which could occur in the samples during cooling.

B. *ThermoElectric Power (TEP)*

The TEP technique has been shown, in many cases,[16–20] to be a performing and sensitive tool to follow the precipitation kinetics in metals due to its high sensitivity to the introduction or departure of atoms from the solid solution. In this technique,[21,22] samples (5 mm wide by 75 mm long) are fixed, at each end, onto a reference metal block (here, pure iron blocks). The two junctions between the reference metal block and the sample are maintained at temperatures T and $T + \Delta T$ (with T = 288 K (15 °C) and ΔT = 10 K). A voltage difference (ΔV), arising from the Seebeck effect, is thus detected at the two junctions. From the measurement of this voltage, the relative TEP (S) of the sample with respect to the TEP of pure iron can be defined at 293 K (20 °C) as follows:

Table I. Composition of the Ferritic Stainless Steel Studied in this Work and Determined by Fluorescence for Most Elements and by Combustion for Light Elements

Elements	Cr	Mo	Nb	Mn	Si	Ni	V	N	C
Wt Pct	18.9	1.86	0.57	0.29	0.26	0.17	0.12	0.02	0.01
At. pct	20.2	1.08	0.34	0.30	0.52	0.16	0.14	0.08	0.04

Alloying elements with a concentration below 0.01 wt. pct were not considered.

$$S = S^*_{sample} - S^*_{pure\ iron} = \frac{\Delta V}{\Delta T},$$

where S^*_{sample} and $S^*_{pure\ iron}$ are the absolute TEP of the sample and of the pure iron blocks, respectively.

The value of this relative TEP is affected by the defects present in the iron matrix of the sample. It can be considered as being the sum of several contributions:

$$S = \Delta S_{ss} + \Delta S_{pre} + \Delta S_{dis},$$

where ΔS_{ss}, ΔS_{dis}, and ΔS_{pre} are the TEP variations due to elements in solid solution, dislocations, or precipitates, respectively.

With regard to the elements in solid solution, they all have a great effect on the TEP of pure iron. This effect depends on their nature and on their concentration in solution. Most of the elements in solution in iron (such as C, N, Mn, Al, Nb, *etc.*) have a negative influence on the TEP of iron,[23] contrary to the case of Cr and Mo which have a positive influence.[18,24] As a consequence, the TEP variation due to the elements in solid solution (ΔS_{ss}) is expected to increase when the elements having a negative effect on the TEP leave the solid solution (for example, to form precipitates).

Concerning the dislocations, they are known to decrease the TEP of iron all the more as their density is high.[25]

Lastly, it has been shown that coarse and incoherent precipitates have no effect on TEP.[16] The consequence is that the TEP variations measured during the precipitation of these precipitates are only due to the departure of alloying elements from the solid solution. However, the formation of small and coherent precipitates may induce a TEP variation, which can be either positive or negative.[16]

C. *SEM and TEM Observations*

SEM was used to visualize the precipitates. Samples for SEM investigations were prepared by grinding and polishing down to 1 μm. The final step of the preparation was performed with a colloidal silica solution to reveal grain boundaries.

TEM investigations were also performed on carbon extraction replicas. Samples were polished and etched for 10 minutes in Villela reactant (10 g picric acid, 50 mL HCl, 1L ethanol). A carbon layer of 30 nm was then deposited on the surface to coat the revealed precipitates. It was detached by dissolving the matrix with the same picric solution. The carbon replicas were then rinsed in three different ethanol baths and retrieved on copper grids before insertion in the TEM. A Jeol 2100 TEM operated at 200 kV was used for bright field (BF) images, energy-dispersive spectroscopy (EDS), and selected area electron diffraction (SAED). EDS was used to differentiate the different types of precipitates and SAED to determine their crystal structure.

D. *Atom probe tomography (APT)*

Atom probe tomography (APT) is a technique allowing the composition of all elements to be measured with the same accuracy, with a near atomic-scale resolution. However, the analyzed volumes are very small, reconstructed volume sizes being of the order of 100 × 100 × 100 nm^3. Therefore, setting the precipitate to be measured in the analyzed volume is still very challenging, in particular when volume fractions are very small. Thanks to recent development in specimen preparation, the use of transmission Kikuchi diffraction (TKD) and focused ion beam (FIB) now gives the possibility to select the location of the analyzed volume with a sub-micro precision. It is thus possible to produce tips samples with Fe_3Nb_3X precipitates localized in their apex.

In the present work, atom probe tomography (APT) was used to measure the composition of the precipitates. The tip samples containing precipitates were prepared by lift up in a FIB system.[26] The different steps of fabrication are illustrated in Figure 1.

E. *Hardness Measurements*

To relate the microstructural changes to mechanical properties, Vickers microhardness measurements were carried out on a Buehler apparatus with a load of 0.5 kg and with a dwell time of 15 seconds.

III. RESULTS

A. *Characterization of the Initial State Obtained After Treatment at 1323 K (1050 °C) and Air Cooling*

First, a SEM characterization of the initial state (Figure 2(a)) was performed. It highlighted that micrometric Nb(C, N) carbides are present, and have nucleated on titanium oxides (coming from some traces of titanium in the industrial product sample). A population of nanoprecipitates, spread as islets was also observed, but they were found to be much too small to be identified by SEM. From TEM EDX and SAED measurements, these precipitates were clearly identified as Fe_3Nb_3X (Figures 2(b) and (c)).

To identify the exact composition of the Fe_3Nb_3X precipitates, APT analyses have been performed on two

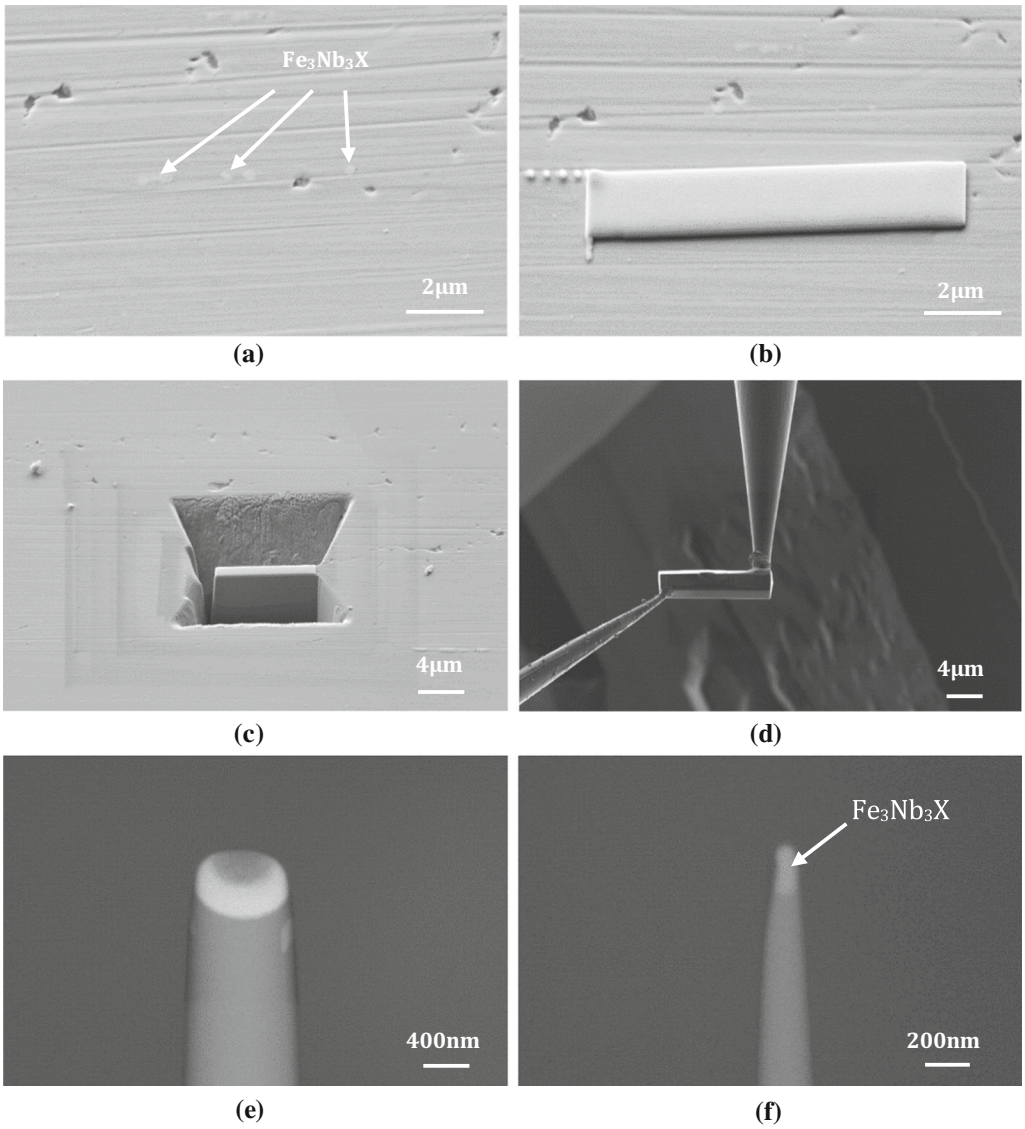

Fig. 1—Lift up performed by Focused Ion Beam (FIB). (*a*) Selection of the precipitates, appearing in bright contrast, and highlighted by white arrows. (*b*) Deposition of platinum to protect the surface during subsequent ion milling. (*c*) Cut out of the surroundings of the platinum deposit and formation of the "wall." (*d*) Separation of the "wall" from the bulk, and welding on a pre-sharpened tip. (*e*) Intermediate step during annular milling of the tip, with part of the platinum protection layer still present. (*f*) Final tip with a Fe_3Nb_3X precipitate at its apex.

distinct precipitates prepared according to the protocol described in Section II–D. Figure 3 presents the distribution of Fe, Nb, C, and N in one of the analyzed precipitates. It can be seen that Fe_3Nb_3X is a mixed precipitate, containing both C and N.

The chemical analysis of the precipitates and of the surrounding matrix is presented in Table II. It has to be noted that the silicon and nitrogen peaks overlap in the APT mass spectra. These two elements are difficult to decorrelate, due to the fact that part of N ions ($^{14}N^{+}$) have the same mass-to-charge ratio as $^{28}Si^{2+}$ ions. Table II gives the Si and N contents after a mass peak deconvolution based on Si natural isotopic ratio.[27] A significant amount of silicon (3.3 at. pct) is found in the precipitates by APT. This result was confirmed by EDX measurements performed on carbon extraction replicas.

With the aforementioned correction on the APT mass spectra, the stoichiometry of the precipitates could be estimated, taking into account that several alloying elements (Cr, Si, and Mo) were also clearly detected in the composition of the precipitates. Considering that iron can be substituted by chromium and niobium by molybdenum and silicon in the Fe_3Nb_3X precipitates,[28] the ratio between (pctFe + pctCr) and (pctNb + pctMo + pctSi) was calculated and it was found to be equal to 0.97. This indicates that the chemical composition of the analyzed precipitates could be of the following type: $(Fe,Cr)_3(Nb,Mo,Si)_3X$. As the precipitates contain both nitrogen (12 at. pct) and carbon (2.9 at. pct) and taking into account the ratio between the different elements, they can be identified as follows:

$$(Fe_{0.81}Cr_{0.19})_3(Nb_{0.85}Si_{0.08}Mo_{0.07})_3(N_{0.8}C_{0.2})$$

A segregation of phosphorus and boron was also observed in the interfacial region between the matrix

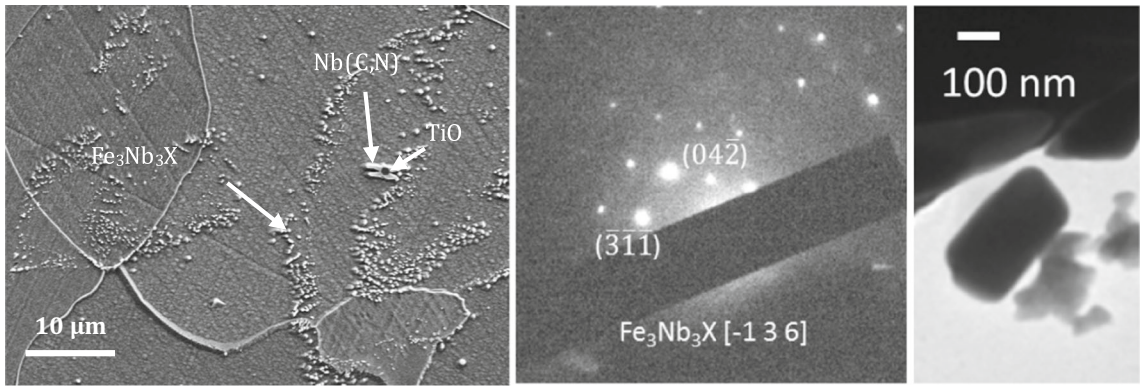

Fig. 2—Initial state observation obtained after air cooling of the sample from 1323 K (1050 °C): (*a*) SEM micrograph revealing the presence of large Nb(C, N) on TiO and smaller precipitates spread as islets later identified as Fe_3Nb_3X, (*b*) TEM SAED of a Fe_3Nb_3X precipitate and (*c*) corresponding TEM Bright Field image.

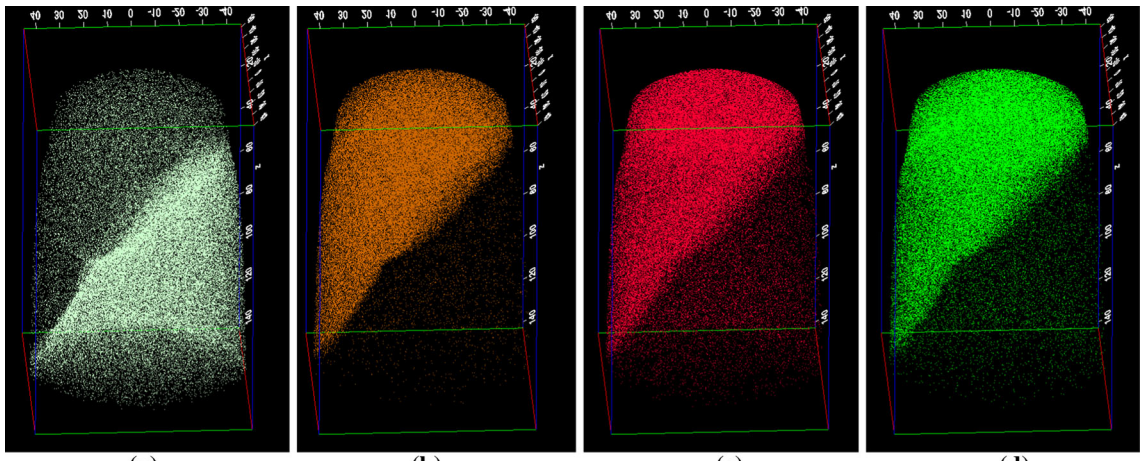

Fig. 3—3D distribution of (*a*) iron, (*b*) niobium, (*c*) carbon, and (*d*) nitrogen atoms in the analyzed sample. Note that only 10, 000 ions per element are represented. The number of represented atoms does not reflect local concentrations.

Table II. Chemical Composition (At. Pct) of the Matrix and of the Precipitate Measured by Atom Probe Tomography

At (Pct)	Fe	Cr	Mo	Si	Nb	V	Ni	Co	Cu	N	C	P
Matrix (APT)	79.6	18	1.12	0.49	0.15	0.13	0.2	0.03	0.02	0.08	0.02	0.03
Precipitate (APT)	33.6	7.79	3.14	3.3	36.2	0.25	0.22	0.02	0.04	12	2.93	0.03
Precipitate (EDS)	31.9	9	3.7	3.7	41.7					10		

The minor elements (O, B, and Ga) were not reported in the table. The uncertainties vary from 0.03 to 0.01 at. pct for the minor elements. For comparison, the chemical composition of the precipitates determined by EDX was also reported in the table.

and the precipitate, as presented in Figure 4. A proxigram (basically a concentration profile with the matrix–precipitate interface as the origin) was calculated (Figure 5). It not only confirms these segregations, but also highlighted a segregation of molybdenum and chromium at the same interface. The slow decrease of molybdenum content from the interface toward the center of the precipitate could reflect a dissolution of the precipitate. As Mo solubility is low in the matrix and its mobility in the precipitate is limited, if the precipitate dissolves, the level of Mo within the precipitate may increase near the interface without homogenizing within the whole precipitate (“snowplow” effect).

B. *Precipitation Kinetics Followed by TEP and Vickers Hardness*

A complete TEP study has been performed on the samples air-cooled from 1323 K (1050 °C) and subsequently, treated from 923 K to 1163 K (650 °C to 890 °C) to determine the range of existence of the different niobium precipitates. Figure 6 plots the evolution of the TEP variation, noted $\Delta S(t,T)$, induced by the thermal treatment at the temperature T for a time t. This variation was defined as follows: $\Delta S(t,T) = S(t,T) - S[t = 1 \text{ minute}, T = 923 \text{ K } (650 \text{ °C})]$, where $S(t,T)$ and $S[t = 1 \text{ minute}, T = 923 \text{ K } (650 \text{ °C})]$ are

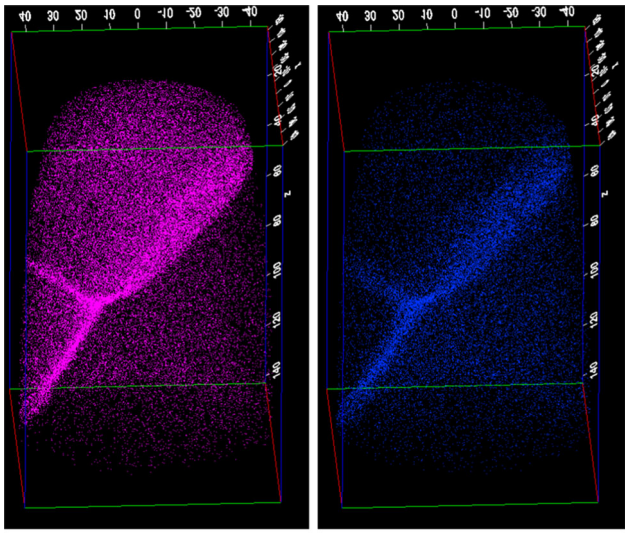

(a) (b)

Fig. 4—3D distribution of (*a*) phosphorus and (*b*) boron atoms in the analyzed volume. A segregation of these two elements is clearly visible in the interfacial region between the matrix and the precipitate. A segregated region is also observed within the precipitate, indicating that possibly two individual adjacent precipitates were analyzed.

the measured TEP values after a time t at temperature T or after $t = 1$ minute at $T = 923$ K (650 °C). It has to be noted that for all samples, the TEP value measured directly after air cooling from 1323 K (1050 °C) was found to be much higher than that measured after $t = 1$ minute at $T = 923$ K (650 °C), contrary to the case where the samples were water-quenched from 1323 K (1050 °C). This was attributed to a modification of the high-temperature microstructure during air cooling, modification which can be suppressed by a short treatment at $T = 923$ K (650 °C).

During aging at 923 K (650 °C), no evolution of TEP is observed from 1 to 60 minutes. This suggests that no major microstructural phenomenon has occurred in the sample. After 20 minutes at 973 K (700 °C), a sharp TEP increase is clearly observed, which tends to indicate that a microstructural evolution has started. A similar behavior is observed for shorter times at 1023 K (750 °C), with a constant increase up to 120 min of heat treatment. When subjected to 1073 K (800 °C) and 1123 K (850 °C), the TEP of the samples first increases, and then reaches a plateau after 20 minutes of heat treatment. This plateau supports the hypothesis that the phenomenon could be finished. A decrease in TEP begins to be observed at 1123 K (850 °C) for longer times, suggesting that another mechanism could start for longer aging times. At 1163 K (890 °C), the increase in TEP is observed from 1 to 10 minutes and is rapidly followed by a TEP decrease.

In order to have a better understanding of the phenomena occurring in the investigated steel, TEP evolution has been followed for longer treatment times at 1123 K (850 °C) and this study was completed with Vickers hardness tests at the same temperature. The results are presented in Figure 7. While TEP increases until 100 minutes of aging, hardness decreases. For longer times, a marked TEP decrease associated with a second hardness decrease is also clearly observed.

C. *SEM and TEM Identification*

From TEP measurements, two particular states were identified and chosen for microstructural characterization: (i) 1 hour at 1073 K (800 °C), corresponding to the plateau reached after the first TEP increase and (ii) 200 hour (12,000 minutes) at 1123 K (850 °C), corresponding to the end of the first TEP decrease.

Figure 8 shows a TEM BF image of the precipitates visible in the first state as well as the corresponding SAED pattern consistent with the presence of precipitates of Fe_2Nb type. These observations were completed with EDS analyses on a population of about 50 precipitates (other than Nb(C, N)) both in the initial state [after air cooling from 1323 K (1050 °C)] and after 1h at 1073 K (800 °C) (Table III). To differentiate the Fe_3Nb_3X and Fe_2Nb precipitates using the EDS spectra, the ratio between (pctFe + pctCr) and (pctNb + pctMo + pctSi) was calculated: when it was found to be close to 1, the precipitates were considered to be of Fe_3Nb_3X type.

These analyses provided evidence that: (i) in the initial state, only Fe_3Nb_3X precipitates are present; (ii) Fe_2Nb precipitates form during aging at 1073 K (800 °C) for 1 hour. Their density is much higher than that of the Fe_3Nb_3X precipitates, which seem to disappear gradually at the expense of the Fe_2Nb precipitates and iii) the ratio (Fe + Cr)/(Nb + Mo + Si) tends to increase in the remaining Fe_3Nb_3X precipitates.

From these observations, one can conclude that the precipitation of Fe_2Nb might be due to the presence of Niobium in solution (0.15pct) in the ferritic matrix in the initial state (Table II) and to the Nb coming from the Fe_3Nb_3X dissolution. These results suggest that the TEP rise shown in the TEP kinetics of Figure 6 could be attributed to the precipitation of Fe_2Nb either directly from the solid solution and/or from pre-existing Fe_3Nb_3X precipitates. Namely, the departure of Nb from the solid solution is expected to lead to a marked TEP increase due to the negative effect of this element when it is in solution in iron.

Figure 9 presents the SEM micrographs obtained after 200 hour (12,000 minutes) at 1123 K (850 °C). Micrometric Nb(C, N) are always detected in the sample, and elongated Fe_2Nb precipitates are found inside ferritic grains as well as at grain boundaries. Inside grains, Fe_2Nb precipitates are aligned and form strings. Their length ranges from 200 to 800 nm, with a thickness of about 80 nm. At the same time, Fe_3Nb_3X precipitates are no longer detected, confirming the fact that they tend to disappear at the expense of Fe_2Nb precipitates.

It was also shown that grain boundaries are decorated with a second phase which appears with a light gray contrast and has a size of few micrometers. An EDS/EBSD analysis (Figure 10) revealed that this phase is a bcc phase, mainly composed of chromium and molybdenum. This Cr, Mo-rich phase corresponds to the

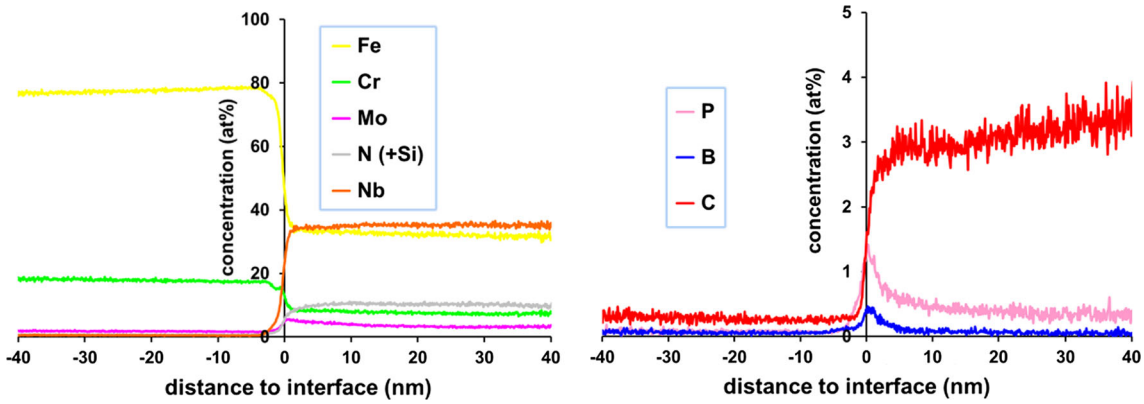

Fig. 5—Proxigrams calculated across the matrix–precipitate interface (matrix on the left, precipitate on the right).

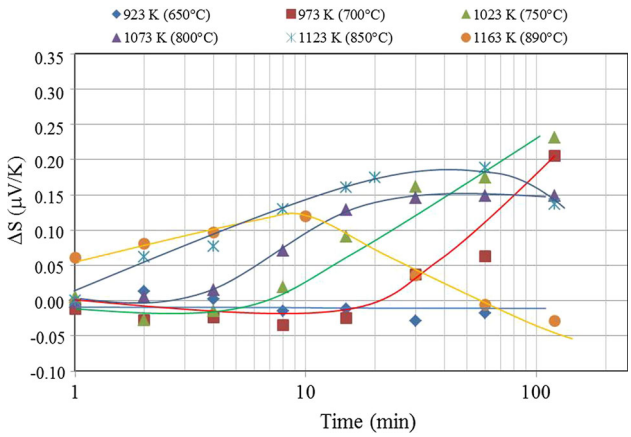

Fig. 6—TEP kinetics reflecting the evolution of $\Delta S(t,T) = S(t,T) - S[t = 1\ \text{min},\ T = 923\ \text{K}\ (650\ ^\circ\text{C})]$ as a function of the treatment time for thermal treatments of 2 h at different temperatures.

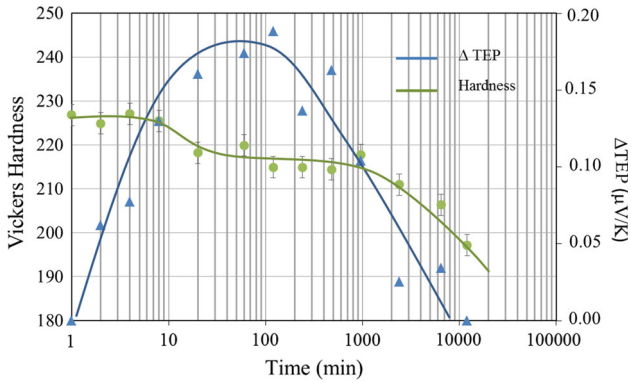

Fig. 7—TEP and Vickers measurements for treatments at 1123 K (850 °C).

χ-phase (a = 0.884 to 0.893 nm), which tends to develop in highly alloyed ferritic stainless steels during aging between 873 K and 1273 K (600 °C and 1000 °C).[13,29] It grows on both sides of the grain boundary and does not contain niobium. However, this element decorates grain boundaries.

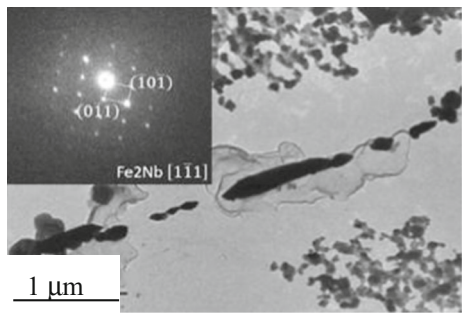

Fig. 8—After 1 h at 1073 K (800 °C) (end of the first TEP increase), TEM BF observation of Fe_2Nb precipitates and corresponding diffraction pattern.

With regard to the TEP measurements, the TEP decrease observed for long aging times at 1123 K (850 °C) (t > 100 minutes) could be due to the precipitation of this phase, since Cr and Mo in solution have a positive influence on TEP. Hence, their departure from the solid solution should lead to a TEP decrease.

IV. DISCUSSION

The first major result of this study concerns the light element of the Fe_3Nb_3X phase. It was shown, using APT, that the Fe_3Nb_3X phase analyzed in the present work contains both carbon and nitrogen with certainty. The measurements performed in this study were made on only two precipitates but they were found to be consistent and repeatable in terms of composition. However, it is important to note that preceding works did not lead to the same conclusion. This is the case of those of Fujita *et al.*[3] who identified a Fe_3Nb_3C phase and those of Malfliet *et al.*[11] who identified a Fe_3Nb_3N phase only. This could be due to the fact that the characterization methods used to determine the chemical composition of the precipitates and to prepare the specimens were different, but this could also come from (i) the differences in the steel chemistry in each study and (ii) the possible dependence of the carbon/nitrogen ratio

Table III. Analysis of the EDS Measurements Performed on a Population of About 50 Precipitates in the Initial State and After 1 h at 1073 K (800 °C)

Type of precipitate	Initial state		1 h at 1073 K (800 °C)			
	Fe_3Nb_3X		Fe_3Nb_3X		Fe_2Nb	
Percentage (pct) [without Nb(C, N)]	100		13		86	
Chemical analysis	Mean Value	SD	Mean Value	SD	Mean Value	SD
N	10.0	10.0	3.6	1.6	1.3	1.3
Si	3.7	0.6	4.8	0.8	7.4	0.7
Cr	9.0	1.2	9.2	0.7	9.7	0.3
Fe	31.9	4.3	38.1	2.1	46.5	2.1
Nb	41.7	6.4	36.9	6.2	21.0	3.2
Mo	3.7	1.2	7.4	2.6	14.9	1.8
(Fe + Cr)/(Nb + Mo + Si)	0.83		0.96		1.30	

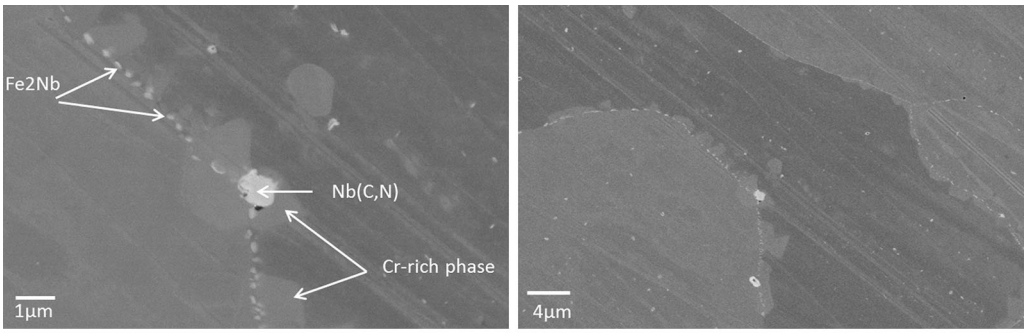

Fig. 9—After 200 h at 1123 K (850 °C) (end of the TEP decrease), the presence of Cr, Mo-rich precipitates at grain boundaries highlighted by SEM observations. (*a*) high magnification, and (*b*) smaller magnification.

with the aging conditions (time and temperature). Further investigations would be necessary to analyze these two effects. Another important conclusion is that other alloying elements (such as Cr, Mo, and Si) were unambiguously detected in the chemical composition of the precipitates.

The APT observations also revealed a segregation of phosphorus and boron at the interphases between the matrix and the precipitates. This phenomenon certainly has an influence on the mechanical behavior of the material, as phosphorus segregation tends to cause an embrittlement of the metal.[29]

From a kinetics point of view, the TEP curves obtained between 923 K (650 °C) and 1163 K (890 °C) showed that two successive microstructural evolutions, associated with a TEP increase followed by a TEP decrease, may occur in this temperature range for short treatment times from 0 to 120 min. For the lower temperatures [T = 973 K, 1023 K, and 1073 K (700 °C, 750 °C, and 800 °C)], only the first microstructural evolution was detected and it was attributed to the departure of niobium from the solid solution due to its precipitation in the form of Fe_2Nb precipitates and also to the progressive dissolution of Fe_3Nb_3X precipitates. As shown in Figure 6, the TEP rise reflecting the precipitation seems to be thermally activated since it is shifted toward short aging times when the aging temperature is increased. At higher temperatures, the precipitation of Fe_2Nb is followed by the formation of the χ-phase, which is a Cr- and Mo-rich phase.

From the TEP kinetics of Figure 6, a time–temperature–precipitation diagram was built for Fe_2Nb precipitates and for the χ-phase (Figure 11). The lines shown in this diagram indicate the time corresponding to the beginning of the precipitation of each phase. The present results are consistent with those of Brown *et al.*[30] who built TTT diagrams for two 25Cr-3Mo-4Ni ferritic stainless steels. These authors showed that the χ-phase, the sigma phase, and the Laves phase may coexist at temperatures between 973 K and 1223 K (700 °C and 950 °C). For their steel with Nb and Ti as stabilizing elements, they showed that the Laves phase precipitates more rapidly than the χ-phase and the sigma phase and that the precipitation nose for Fe_2Nb is around 1123 K (850 °C). Other results obtained by Ma *et al.*[13] on a Fe-26Cr-4Mo-2Ni ferritic stainless steel stabilized with Nb and Ti showed the coexistence of the χ-phase, the sigma phase, and the Laves phase during an isothermal treatment at 800 °C. In our case, the precipitation of the sigma phase was not detected after 200 hours at 1123 K (850 °C). However, it could occur for longer aging times leading to an embrittlement of the steel.

From a mechanical point of view, the two microstructural evolutions, highlighted by TEP, were found to be

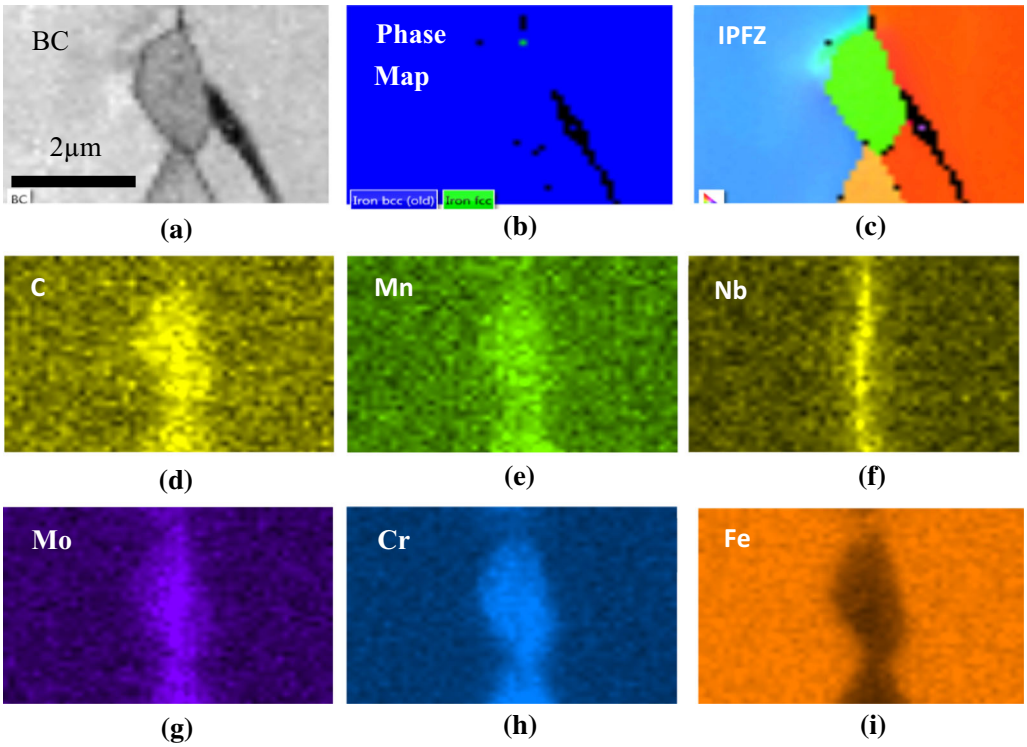

Fig. 10—Bcc Cr-Mo-rich precipitates observed at grain boundary after 12,000 min of aging at 1123 K (850 °C): (*a*) Band Contrast (BC, also known as Index Quality IQ), (*b*) Phase Map revealing the bcc structure of the precipitates, (*c*) Inverse Pole Figure perpendicular to the surface (IPFZ map), (*d*), (*e*), (*f*), (*g*) (*h*) and (*i*) are carbon, manganese, niobium, molybdenum, chromium, and iron EDS maps, respectively.

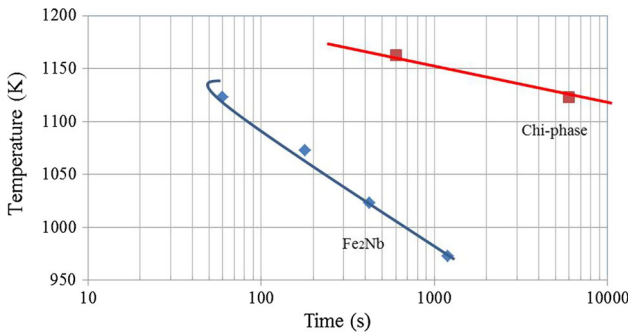

Fig. 11—TTT diagram for Fe_2Nb and χ-phase plotted from the TEP kinetics of Fig. 6 for a temperature between 923 K and 1163 K (650 °C and 890 °C).

associated with two successive decreases in hardness. The first decrease is less pronounced that the second decrease and can be attributed to the matrix softening due to its depletion in Niobium and/or to the coarsening of the Fe_2Nb precipitates which may occur during the first minutes of aging at 1123 K (850 °C). This is consistent with the works of Miyazaki *et al.*[4] and Sim *et al.*[5] which showed that the coarsening of the Fe_2Nb particles leads to a marked decrease in the high-temperature proof strength of Nb-added ferritic stainless steels at 973 K (700 °C).

The second decrease in hardness seems to be attributed to the replacement of the Fe_3Nb_3X by the χ-phase, which is considered to be detrimental to the steel properties.[31] The decrease in hardness associated with the formation of this phase could be attributed to the matrix softening due to its depletion in molybdenum.

V. CONCLUSION

The precipitation occurring in a Nb-stabilized ferritic stainless steel, containing initially Nb(C, N) carbonitrides and Fe_3Nb_3X precipitates, was investigated during aging treatments performed between 923 K and 1163 K (650 °C and 890 °C) by combining different techniques (TEP, SEM/TEM), in order to obtain complementary information about the kinetics and the morphology of the newly formed precipitates. Furthermore, the chemical composition of the initial Fe_3Nb_3X precipitates was analyzed using APT in order to determine the nature of the light element.

The following conclusions have been drawn:

1. Fe_3Nb_3X precipitates have been successfully characterized by APT. Two light elements (C and N) were found to coexist in the precipitates. Furthermore, other alloying elements (such as Cr, Mo, and Si) were clearly detected inside the precipitates. This led us to propose the following chemical composition for these precipitates: $(Fe_{0.81}\ Cr_{0.19})_3\ (Nb_{0.85}\ Si_{0.08}\ Mo_{0.07})_3\ (N_{0.8}\ C_{0.2})$.
2. A segregation of phosphorus and boron was observed by APT in the interfacial region between the Fe_3Nb_3X precipitates and the matrix. This could

play a role on the mechanical properties of the steel, as phosphorus segregation is known to cause embrittlement of metals.

3. Precipitation kinetics for treatments from 923 K to 1163 K (650 °C to 890 °C) were investigated with TEP and TEM. From 973 K to 1163 K (700 °C and 890 °C), a rise in TEP was observed and attributed to the formation of Fe_2Nb precipitates at the expense of the pre-existing Fe_3Nb_3X precipitates. For treatments at 1123 K (850 °C) and 1163 K (890 °C), this rise in TEP was found to be followed by a TEP decrease. SEM and TEM measurements showed that this phenomenon corresponds to the formation of the χ-phase (mainly composed of chromium and molybdenum) at grain boundaries. This result was found to be consistent with the TEP measurements, as the departure of chromium and molybdenum from the solid solution is expected to lead to a TEP decrease.
4. The TEP technique appeared to be appropriate to follow the precipitation in Nb-stabilized ferritic stainless steels. From the TEP kinetics obtained between 923 K and 1163 K (650 °C and 890 °C), a time–temperature–precipitation diagram was built for the investigated steel.

ACKNOWLEDGMENTS

Thanks are due to the Clym (Consortium Lyonnais de Microscopie) for access to the 2100 microscope, and to N. Blanchard for his assistance with the TEM. The work has received funding from the French CNRS-CEA *METSA network* for FIB sample preparation and Atom Probe measurements.

REFERENCES

1. J.H. Schmitt: *Key Eng. Mater.*, 2002, vols. 230–232, pp. 17–22.
2. N. Fujita, K. Ohmura, M. Kikuchi, T. Suzuki, S. Funaki, and I. Hiroshige: *Scr. Mater.*, 1996, vol. 35 (6), pp. 705–10.
3. N. Fujita, K. Ohmura, and A. Yamamoto: *Mater. Sci. Eng. A*, 2003, vol. 351, pp. 272–81.
4. A. Miyazaki, K. Takao, and O. Furukumi: *ISIJ Int.*, 2002, vol. 42 (8), pp. 916–20.
5. G.M. Sim, J.C. Ahn, S.C. Hong, K.J. Lee, and K.S. Lee: *Mater. Sci. Eng. A*, 2005, vol. 396, pp. 159–65.
6. F. Vieira Braga, D. Pérez Escobar, T.J. Ávila Reis, N.J. de Lucinda Oliveira, and M.S. Andrade: *J. Mater. Res. Technol.*, 2016, vol. 5 (1), pp. 92–99.
7. F. Chassagne, J.D. Mithieux, and J.H. Schmitt: *Steel Res. Int.*, 2006, vol. 77 (9–10), pp. 680–85.
8. Y. Shan, X. Luo, X. Hu, and S. Liu: *J. Mater. Sci. Technol.*, 2011, vol. 27 (4), pp. 352–58.
9. C.S. Tedmon, D.A. Vermilyea, and J.H. Rosolowski: *J. Electrochem. Soc.*, 1971, vol. 118 (2), pp. 192–202.
10. X. Huang, D. Wang, and Y. Yang: *J. Iron Steel Res.*, 2015, vol. 22 (11), pp. 1062–68.
11. A. Malfliet, W. Van den Broek, F. Chassagne, J.D. Mithieux, B. Blanpain, and P. Wollants: *J. Alloys Compd*, 2011, vol. 509, pp. 9583–88.
12. A. Malfliet, F. Mom Piou, and F. Chassagne: *Metall. Mater. Trans. A*, 2011, vol. 42A, pp. 3333–43.
13. L. Ma, S.S. Hu, and J.Q. Shen: *Ironmak. Steelmak.*, 2016, vol. 43 (10), pp. 752–57.
14. D. Boyd, Z. Yao, Application of modern transmission electron microscopy (TEM) techniques to the study of phase transformations in steels, Phase Transformations in Steels: diffusionless transformations, high strength steels, modelling and advanced analytical techniques, Volume 2 in Woodhead Publishing Series in Metals and Surface Engineering, pp. 507–31, 2012.
15. G.G. Hembree, J.S. Drucker, F.C.H. Luo, M. Krishnamurthy, and J.A. Venables: *Appl. Phys. Lett.*, 1991, vol. 58 (17), pp. 1890–92.
16. J. Pelletier, G. Vigier, J. Merlin, P. Merle, F. Fouquet, and R. Borrelly: *Acta Metall.*, 1984, vol. 32, pp. 1069–78.
17. N. Lavaire, V. Massardier, and J. Merlin: *Scripta Mater.*, 2004, vol. 50, pp. 131–35.
18. M. Houzé, X. Kléber, F. Fouquet, and M. Delnondedieu: *Scr. Mater.*, 2004, vol. 51 (12), pp. 1171–76.
19. M. Perez, F. Perrard, V. Massardier, X. Kléber, A. Deschamps, H. De Monestrol, P. Pareige, and G. Covarel: *Philos. Mag.*, 2005, vol. 85, pp. 2197–10.
20. M. Perez, V. Massardier, and X. Kleber: *Int. J. Mat. Res.*, 2009, vol. 100 (10), pp. 1461–65.
21. F. Blatt, P. Shroeder, C. Foiles, and D. Creig: *Thermoelectric Power of Metals*, Springer, New York, 1976.
22. R. Borrely and J.L. Bouvier-Volaille: *Trait. Therm.*, 1988, vol. 221, pp. 43–45.
23. A. Brahmi, PhD thesis, Institut National des Sciences Appliquées de Lyon, France, 1993.
24. M. Houzé, PhD thesis, Institut National des Sciences Appliquées de Lyon, France, 2002.
25. N. Lavaire, V. Sardoy, and J. Merlin: *Scr Mater.*, 2001, vol. 44, pp. 553–59.
26. K. Thompson, D. Lawrence, D.J. Larson, J.D. Olson, T.F. Kelly, and B. Gorman: *Ultramicroscopy*, 2007, vol. 107, pp. 131–39.
27. J. Martin, A. Martinavicius, S. Bruyère, H.P. Van Landeghem, C. Gendarme, F. Danoix, R. Danoix, A. Redjaimia, T. Grosdidier, and T. Czerwiec: *J. Alloys Compod*, 2016, vol. 683, pp. 418–26.
28. J.D. Redmond, P.J. Grobner, and V. Biss: *J. Met.*, 1981, vol. 33 (2), pp. 19–25.
29. H.K.D.H. Bhadeshia and D.-W. Suh: *Ironmak. Steelmak.*, 2015, vol. 42, pp. 259–67.
30. E.L. Brown, M.E. Burnett, P.T. Purtscher, and G. Krauss: *Metall. Mater. Trans. A*, 1983, vol. 14A, pp. 791–800.
31. A.F. Padilha, R.L. Plaut, P.R. Rios: Stainless steels heat treatment (Chapter 12). In: Totten GE, editor. Steel Heat Treatment. CRC Press: Boca Raton.